Fast, faithful, frequency-domain effective-one-body waveforms for compact binary coalescences

Rossella Gamba, Sebastiano Bernuzzi, and Alessandro Nagar

Phys. Rev. D **104**, 084058 — Published 14 October 2021

DOI: 10.1103/PhysRevD.104.084058

Fast, faithful, frequency-domain effective-one-body waveforms for compact binary coalescences

Rossella Gamba[1], Sebastiano Bernuzzi[1], and Alessandro Nagar[2,3,4]
[1] *Theoretisch-Physikalisches Institut, Friedrich-Schiller-Universität Jena, 07743, Jena, Germany*
[2] *Centro Fermi - Museo Storico della Fisica e Centro Studi e Ricerche Enrico Fermi, Rome, Italy*
[3] *INFN Sezione di Torino, Via P. Giuria 1, 10125 Torino, Italy and*
[4] *Institut des Hautes Etudes Scientifiques, 91440 Bures-sur-Yvette, France*
(Dated: September 22, 2021)

The inference of binary neutron star properties from gravitational-wave observations requires the generation of millions of waveforms, each one spanning about three order of magnitudes in frequency range. Thus, waveform models must be efficiently generated and, at the same time, be faithful from the post-Newtonian quasi-adiabatic inspiral up to the merger regime. A simple solution to this problem is to combine effective-one-body waveforms with the stationary phase approximation to obtain frequency-domain multipolar approximants valid from any low frequency to merger. We demonstrate that effective-one-body frequency-domain waveforms generated in post-adiabatic approximation are computationally competitive with current phenomenological and surrogate models, (virtually) arbitrarily long, and faithful up to merger for any binary parameter. The same method can also be used to efficiently generate intermediate mass binary black hole inspiral waveforms detectable by space-based interferometers.

Gravitational-wave (GW) analyses of binary neutron star (BNS) signals rely on matched filtering techniques and waveform models to infer the source properties from observations. The inspiral-to-merger signal is observable in the ground-based interferometer frequency band for minutes, that correspond to thousands of inspiralling cycles to merger [1, 2]. Waveform templates must model the signal phase evolution over a frequency range spanning from few Hz to kHz [3–5]. Further, due to the large number ($\sim 10^7$) of waveforms needed to explore the posterior distribution of the parameters, such models also need to be computationally efficient. Similar issues arise for the computation of waveforms for binary black hole (BBH) inspirals, that are observable in the mHz to Hz regime with space-based interferometers for binary masses $\sim(100-10^5)\mathrm{M}_\odot$ [6–8]. In this case, the waveforms efficiency requirements are even more demanding as the binary remains in band for days to years, corresponding to up to millions inspiralling cycles [9].

Analytical post-newtonian (PN) approximants are quick to evaluate and can be turned into closed-form frequency-domain templates by applying the stationary phase approximation (SPA) [10–14]. While PN approximants become unfaithful as the binary motion becomes nonadiabatic (high velocities regime), the domain of validity of the SPA itself was proven to be accurate at least up to frequencies corresponding to the last stable orbit, e.g. [11, 13]. Such a validity interval corresponds to binaries with total mass $M \lesssim 13\mathrm{M}_\odot$ in the ground-based interferometers range, and it is large enough to cover BNS and - possibly - also light BHNS or BBH systems. From the trivial scaling of the waveform with the binary mass, it follows that the SPA is valid also for the inspiral of stellar and intermediate-mass BBH in the LISA band [6, 7].

Beyond PN approximants, effective-one-body (EOB) [15–27] and phenomenological (Phenom) [28–33] models describe the waveform from the early inspiral up to merger [and ringdown, if dealing with BBH systems], but are in general computationally less efficient. In particular, EOB models need to evolve the dynamics of the system by solving the Hamilton equations. This process can be very expensive when the ODEs are integrated *numerically* for thousands of orbits. Moreover, while Phenom models output frequency domain (FD) waveforms, EOB models natively generate time domain (TD) waveforms, so that an additional Fourier transform is needed, with the related performance loss. Reduced-order-quadrature [34–36] and reduced-order modeling techniques offer a solution to the issue of performances. The latter can be used to produce fast surrogate models from a training set of waveforms [37–43]. However, surrogate waveforms are limited by the length and parameters span of the training set and they must be regenerated if the baseline model is varied.

EOB waveforms can alternatively be speeded up using dedicated analytical methods. The postadiabatic method gives an approximate, iterative solution for the EOB Hamiltonian dynamics [44–47] that is valid for any binary system evolving along quasi-circular orbits. Such a simple, physically motivated technique was shown to allow for the computation of BNS TD waveforms from frequencies as low as a few Hz in a matter of tens of milliseconds. However, such waveforms still need to be translated into the FD. In this work we apply the SPA to EOB waveforms in order to obtain computationally inexpensive frequency-domain templates. The FD waveforms obtained this way are suitable for the GW data analysis of BNS signal up to merger and of long BBH inspiral for masses $\gtrsim 1000\mathrm{M}_\odot$. We call $M \equiv m_1 + m_2$ the binary mass, where $m_{1,2}$ are the individual masses;

$q \equiv m_1/m_2 \geq 1$ is the mass ratio, $\nu \equiv m_1 m_2/M^2$ the symmetric mass ratio, and $\chi_{1,2} \equiv S_{1,2}/m_{1,2}^2$ the dimensionless individual spins (anti)aligned with the orbital angular momentum; $\Lambda_{1,2}$ are the individual quadrupolar tidal polarizability parameters [48–51], and $\tilde{\Lambda}$ the reduced tidal parameter [52–54]. Geometric units $G = c = 1$ are employed unless stated differently.

The FD extension of a given a TD EOB waveform is computed by applying the SPA to the multipolar TD modes $h_{\ell m}(t) = a_{\ell m} e^{\mathrm{i}\phi_{\ell m}(t)}$ to obtain

$$\tilde{h}^{\mathrm{SPA}}_{\ell m} = \tilde{A}^{\mathrm{SPA}}_{\ell m} e^{i\Psi^{\mathrm{SPA}}_{\ell m}} = \frac{a_{\ell m}\left(t_f\right)}{\sqrt{\ddot{\phi}_{\ell m}\left(t_f\right)/2\pi}} e^{\mathrm{i}\left[\psi_f\left(t_f^{\ell m}\right)-\pi/4\right]}\,, \tag{1}$$

with $\psi_f(t) \equiv 2\pi f t - \phi(t)$ and where t_f denotes the stationary point of $\psi_f(t)$. The two GW polarizations in FD are then computed by combining the multipolar modes with spin-weighted spherical harmonics in a standard way. The TD-to-FD computation is straightforward, the key technical details in our implementations are given in the Supplemental Material. We apply the SPA to TD `TEOBResumS`, a state-of-the-art effective EOB approximant for spin-aligned binaries [26, 46, 55–58], that includes resummed tidal interactions from PN and gravitational-self force results [45, 46, 59]. The resulting FD `TEOBResumSPA` model retains the same accuracy as the TD `TEOBResumS` up to merger for any BNS signal, and for waveforms with initial frequency $f_0 \lesssim 15$ Hz its speed is comparable to that of other commonly used tidal waveform approximants.

Figure 1 (left panel) shows the FD phasing of a fiducial BNS waveform for a $(M/M_\odot, q, \chi_1, \chi_2, \tilde{\Lambda}) = (2.8, 1, 0, 0, 400)$ system, sampled at 8192 Hz with initial frequency $f_0 = 20$ Hz and computed either Fourier transforming the TD `TEOBResumS` (solid black line) or using the SPA (dashed red line). `TEOBResumSPA` correctly reproduces the waveform of the original TD model from the early inspiral up to merger; the accumulated total phase difference amounts to $\sim$0.1 to merger (vertical line).

We quantitatively assess the faithfulness of `TEOBResumSPA` against `TEOBResumS` on a sample of 10^4 waveforms from BNS with $m_{1,2} \in [1, 2.5]M_\odot$, $\chi_{1,2} \in [-0.5, +0.5]$ and $\Lambda_{1,2} \in [10, 5000]$. Since the masses and the tidal parameters are sampled separately, no specific equation of state is imposed. We recall that the mismatch $\bar{\mathcal{F}}$ (and the match $\mathcal{F}$) between two waveforms (h, s) is defined by

$$\bar{\mathcal{F}} \equiv 1 - \mathcal{F} = 1 - \max_{t_c,\phi_c} \frac{(h,s)}{\sqrt{(h,h)(s,s)}}\,, \tag{2}$$

where t_c and ϕ_c denote the time and phase at coalescence, and the Wiener scalar product associated to the power-spectral density (PSD) of the detector, $S_n(f)$, is

$$(h,s) = 4\,\Re \int \frac{\tilde{h}^*(f)\tilde{s}(f)}{S_n(f)}\,\mathrm{d}f. \tag{3}$$

Since the detection rate loss scales as $(1-(1-\bar{\mathcal{F}})^3)$, $\bar{\mathcal{F}} \leq 0.035$ is usually usually regarded to be satisfactory for detection purposes [60]. However, the value of $\bar{\mathcal{F}}$ does not depend on the signal-to-noise ratio (SNR) and does not account properly for statistical fluctuations (or lack thereof) due to the background noise. An approximate criterion to determine if two waveforms are faithful is given by the condition [60–62]

$$\bar{\mathcal{F}} \leq \bar{\mathcal{F}}_{\mathrm{SNR}} \equiv \frac{D}{2\,\mathrm{SNR}^2}\,, \tag{4}$$

where $D = 6$ is the number of intrinsic parameters. This means that we require for the systematical errors introduced by the SPA approximation to be smaller than the expected statistical fluctuations. The threshold SNRs chosen in Eq. (4) are 13, 33 and 80. The first two values mimic the SNRs of the two BNSs observed by LIGO/Virgo in O3 and O2 respectively, while the last value can be reached for GW170817-like event at design sensitivity or in third generation detectors [63]. The above numbers lead to the threshold unfaithfulnesses of $\bar{\mathcal{F}}_{13} \approx 1.8 \times 10^{-2}$, $\bar{\mathcal{F}}_{33} \approx 2.7 \times 10^{-3}$ and $\bar{\mathcal{F}}_{80} \approx 5 \times 10^{-4}$.

Figure 1 (right panel) shows the matches between `TEOBResumS` and `TEOBResumSPA` for our BNS sample with a starting frequency $f_0 = 20$ Hz and assuming the Advanced LIGO `ZeroDetunedHighPower` PSD [64]. We find that more than 99% of total mismatches lie below the most conservative threshold $\bar{\mathcal{F}}_{80}$. The worst performances ($\bar{\mathcal{F}} \sim 5.2\times10^{-4}$ and $\bar{\mathcal{F}} \sim 5.4\times10^{-4}$) are obtained for two cases with equal mass configurations and large $\tilde{\Lambda}$ values ($\tilde{\Lambda} > 2000$). Note however that the dependence of the mismatch on the effective tidal parameter is much weaker that that on the mass ratio.

While the loss of accuracy with respect to the TD EOB is negligible, the speed up given by the SPA is significant. The computational performance of our FD EOB waveform is assessed by comparing the evaluation times of `TEOBResumSPA` waveforms to that of other FD BNS approximants. In particular, we compare to PN `TaylorF2`, considered here with a 3.5PN-accurate description of the point-mass phasing and 7PN-accurate tidal effects; `IMRPhenomDNRTidal` [65, 66], a phenomenological approximant for aligned-spin binaries augmented by the `NRTidal` phase and amplitude prescriptions; `SEOBNRv4Tsurrogate` [41], a FD surrogate of the EOB tidal model of Ref. [67, 68]; `SEOBNRv4_ROM_NRTidal` a FD reduced-order model of the EOB model [22] augmented by the `NRTidal` phasing.

We simulate the fiducial BNS coalescence with varying initial frequency $f_0 = (5, 10, 15, 20, 25, 30)$ Hz and uniform frequency spacing $\Delta f = (1/8192, 1/2048, 1/512, 1/256, 1/128, 1/128)$ Hz, and compute the average generation time to $f_{\max} = 2048$ Hz over ten repetitions for each of the approximants listed above. The timing results are shown in Fig. 2. `TEOBResumSPA` generation times

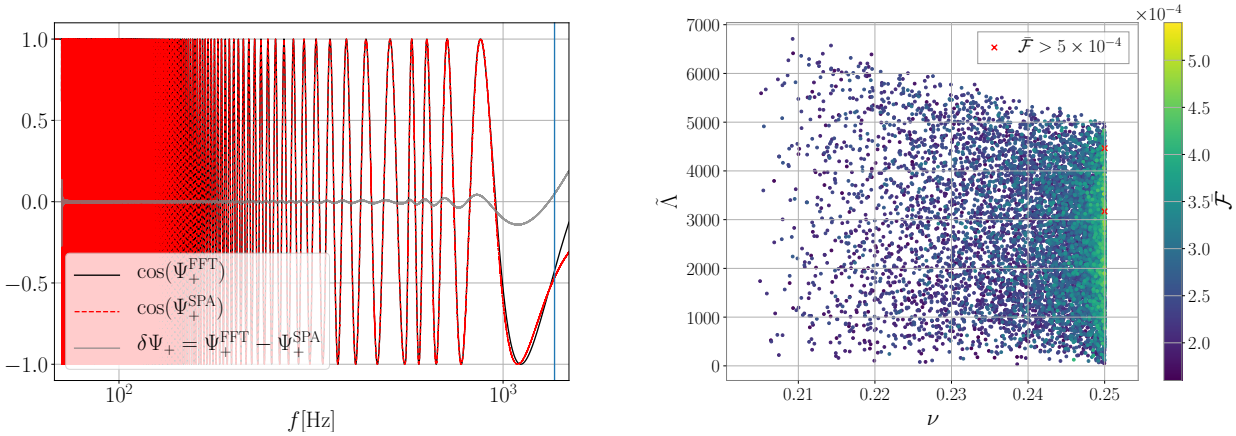

FIG. 1. Left: comparison between the (cosines of) the frequency domain phase of the $\tilde{h}_+$, computed with `TEOBResumSPA` and the FFT of `TEOBResumS` for a $q = 1$, $M = 2.8M_\odot$, $\chi_{1,2} = 0.1$ and $\tilde{\Lambda} = 400$ system. The phase difference between the two models remains below $\delta\Psi_+ \lesssim 0.1$ rad to merger (blue vertical line). Right: Unfaithfulness between `TEOBResumSPA` and Fourier-transformed `TEOBResumS`, computed for 10^4 binary systems with varying spins, masses and component tidal parameters. Waveforms are computed from an initial frequency of 20 Hz, and matches computed between 20 Hz and 2 kHz. We find that only two values (denoted with red crosses) lie below the SNR 80 threshold of Eq.(4). The mismatch values found, however, are still $\bar{\mathcal{F}} \sim 10^{-4}$).

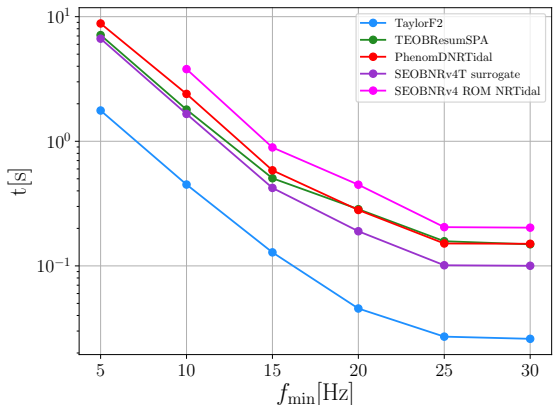

FIG. 2. Generation times of different BNS waveforms averaged over 10 repetitions as a function of initial frequency for a fiducial BNS with $(M/M_\odot, q, \chi_1, \chi_2, \tilde{\Lambda}) = (2.8, 1, 0, 0, 400)$. Below 15 Hz `TEOBResumSPA` is comparable to the `SEOBNRv4Tsurrogate` and `IMRPhenomDNRTidal` models and ∼2 times faster than `SEOBNRv4_ROM_NRTidal`.

for $f_0 \gtrsim 15$ Hz, in green, are comparable to those of `IMRPhenomDNRTidal`, a factor two smaller than `SEOBNRv4_ROM_NRTidal` and up to a factor ten slower than `TaylorF2`. For starting frequencies $f_0 < 15$ Hz, `TEOBResumSPA` is comparable to `SEOBNRv4Tsurrogate` and `IMRPhenomDNRTidal`, and at least a factor two faster than `SEOBNRv4_ROM_NRTidal`.

Further tests indicate that `TEOBResumSPA` generation times display a small variance over a large parameter space ($m_{1,2} \in [1, 2.5]M_\odot, \chi_{1,2} \in [-0.5, 0.5], \Lambda_{1,2} \leq 5000$).

TABLE I. Source properties of GW170817 [69] and GW190425 [70]. The new measurements are quoted through the median and 90% credible intervals of the parameters' marginalized one-dimensional posterior distributions. The estimates found with `TEOBResumSPA` are compared to the LIGO-Virgo results. The `TEOBResumSPA` anaysis is performed up to ∼ 1kHz following [63] in order to minimize waveform systematics; this approach is the main responsible for the different estimate of $\tilde{\Lambda}$ when compared to [69].

	GW170817		GW190425	
	LVC [69]	`TEOBResumSPA`	LVC [70]	`TEOBResumSPA`
$1/q$	0.73-1.00	$0.89^{+0.10}_{-0.2}$	0.8-1.0	$0.9^{+0.1}_{-0.1}$
$\mathcal{M}$ $[M_\odot]$	$1.1975^{+0.0001}_{-0.0001}$	$1.1976^{+0.0001}_{-0.0001}$	$1.4868^{+0.0003}_{-0.0003}$	$1.4868^{+0.0005}_{-0.0005}$
$\tilde{\Lambda}$ [a]	300^{+500}_{-190}	530^{+350}_{-310}	≤ 600	≤ 550
$\chi_{\rm eff}$	$0.00^{+0.02}_{-0.01}$	$0.00^{+0.02}_{-0.01}$	$0.01^{+0.01}_{-0.01}$	$0.01^{+0.01}_{-0.01}$
D_L [Mpc]	39^{+7}_{-14}	42^{+6}_{-13}	159^{+69}_{-72}	180^{+61}_{-77}

[a] The values of $\tilde{\Lambda}$ are quoted after reweighting to flat in $\tilde{\Lambda}$ prior. Note however that the procedures followed for the reweighting of the GW170817 and GW190425 posteriors are different, for consistency with Sec. 3D of [69] and App. F.1 of [70].

This is due to the fact that the largest computational burden of the approximant lies in the uniform-frequency interpolation of the multipoles $h_{\ell m}$, which is approximately independent of the binary parameters. A further speedup would be simply obtained by considering a non-uniform frequency grid for the likelihood computation, see e.g. [72, 73]. We also stress that since the SPA is an analytical procedure, it can be applied to any waveform, and is valid for any initial frequency and any binary parameters. This is in contrast to waveform models based on surrogates or machine learning [74], that are

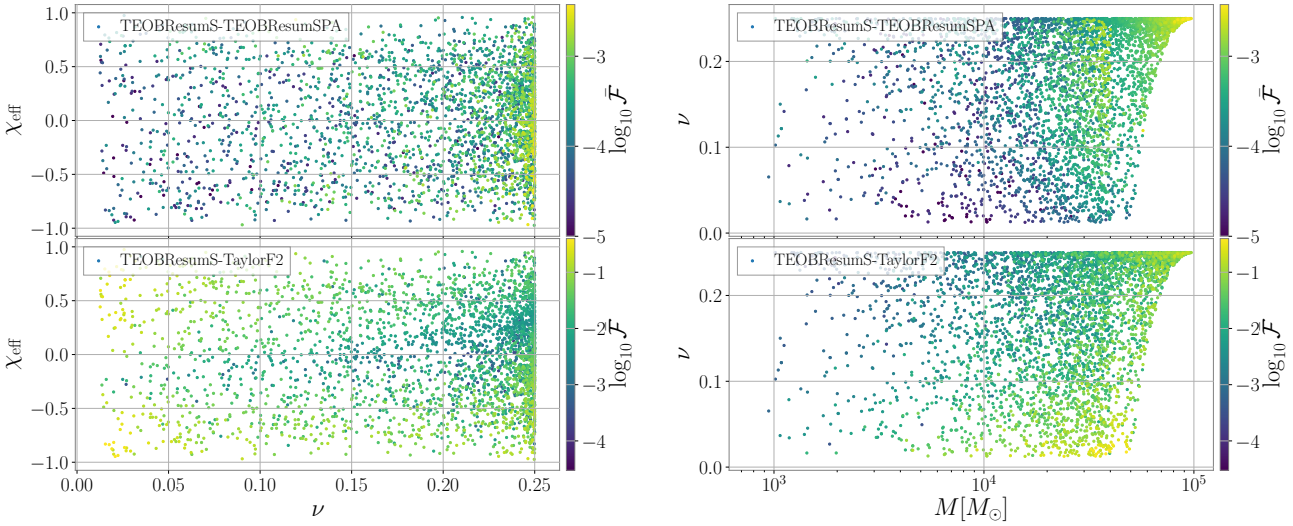

FIG. 3. Mismatches $\bar{\mathcal{F}}$ between TD `TEOBResumS` and `TEOBResumSPA` (top) or the 3.5PN-accurate `TaylorF2` (bottom) on the frequency range $[0.02, 1]$ Hz obtained via Eq. (2) with the LISA noise curve [71]. Left column: `TaylorF2` is effectual only for moderate values of the effective spin parameter $\chi_{\rm eff} \equiv S_1/(m_1 M) + S_2/(m_2 M)$. Right column: for moderately large mass ratios ($\nu \leq 0.1$, corresponding to $q \gtrsim 7.8$) and massive ($M > 10^4 \mathrm{M}_\odot$) BBH systems, mismatches between `TEOBResumS` and `TaylorF2` become large, reaching $\bar{\mathcal{F}} \sim 0.1$.

limited by the length and parameter range of the training set. Note for example that it is not possible to generate `SEOBNRv4_ROM_NRTidal` waveform at dimensionless frequencies below $Mf = 9.85 \times 10^{-5}$, which is the minimal frequency of the surrogate. Thus, the flexibility of the SPA method applied to EOB waveforms has an obvious advantage, in particular in view of the continuous and rapid development of EOB models.

We demonstrate the use of `TEOBResumSPA` in GW parameter estimation by performing the analysis of GW170817 [69, 75–77] and GW190425 [70]. We employ the `pbilby` [78, 79] and `dynesty` [80] parameter estimation infrastructures and the same setup of [63], to which we refer for all technical details. These analyses run in two-to-three days time on 4×16 CPUs. For comparison, the same GW170817 analysis, performed with the phenomenological `IMRPhenomPv2NRTidal` [29, 66] approximant with an identical setup, required longer than 5 days to complete. Results are listed in Table I, and are consistent with LIGO-Virgo analyses. The measurement of $\tilde{\Lambda}$ differs from the LIGO-Virgo one mainly because of our conservative choice of the sampling rate, as discussed in [63].

Fast and accurate EOB waveforms will be crucial for the analysis of high-SNR BNS signals as those detectable by the Einstein Telescope or Cosmic Explorer [81–84]. Recent work has demonstrated that at SNR $\gtrsim$80 the systematics among advanced BNS approximants shown in Fig. 2 will be the dominant source of error in the measurements of tidal effects [63]. High-precision measurements for constraining the NS equation of state will require new numerical-relativity informed tidal EOB models [4, 67] or new closed-form representations of the tidal sector [66]. Ongoing work in these directions based on the EOB SPA method will be presented elsewhere.

The EOB SPA waveform can be used to compute accurate inspiral waveforms of intermediate-mass BBH that will be observed by LISA in the mHz to Hz regime [6] and possibly in the dHz regime by planned space-based detectors as DECIGO [7, 8, 85]. Besides PN and EOB approximants, no other modeling technique is available for this inspiral-to-late-inspiral regime [86]. We focus on LISA sources with total masses $\sim 10^3 - 10^5 \mathrm{M}_\odot$ and mass ratio up to $q \sim 80$ [87]. For such systems, the ringdown is either outside the LISA band or, if within the considered frequency range, it carries negligible SNR with respect to the inspiral. Figure 3 compares $\sim 10^4$ mismatches between `TEOBResumS`–`TEOBResumSPA` with `TEOBResumS`–`TaylorF2` (at 3.5PN accuracy) computed with the LISA noise curve [71]. The right column focuses on the (ν, M) dependence; the effect of spin is described by $\chi_{\rm eff} \equiv S_1/(m_1 M) + S_2/(m_2 M)$. The figure highlights that `TaylorF2` becomes more and more inaccurate when: (i) $M \gtrsim 10^3 M_\odot$; (ii) when $q \gtrsim 8$ ($\nu \lesssim 0.0988$) and (iii) when spin magnitudes are not moderate. Specifically, the worst `TEOBResumS` – `TaylorF2` mismatch ($\bar{\mathcal{F}} = 0.397$) corresponds to $(M/M_\odot, q, \chi_1, \chi_2) = (7670, 55, -0.84, -0.62)$, and detection losses up to 78%. In addition, we use again Eq. (4), and consider SNR of 20 and 100 [6, 88] to find threshold mismatches of $\bar{\mathcal{F}}_{20} = 5 \times 10^{-3}, \bar{\mathcal{F}}_{100} = 2 \times 10^{-4}$ for $D = 4$. `TEOBResumS`-`TEOBResumSPA` mismatches always lie below the lower threshold $\mathcal{F}_{20}$, while $\approx$ 43%

of the simulated signals also satisfy the stricter requirement with $\bar{\mathcal{F}}_{100}$. On the contrary, 59% of the PN waveforms are not faithful at SNR 20, and 42% of them correspond to systems with $q > 8$. Therefore, `TaylorF2` is not a robust choice for parameter estimation of these BBH sources. The discrepancy between PN and EOB further increases considering higher frequencies; the analysis of intermediate-mass BBH in the the dHz regime (e.g. DECIGO band) will require fast and accurate FD EOB models like `TEOBResumSPA` (see Supplementary Material).

In summary, the EOB SPA method proposed here will crucially support both ground-based and spaced-based observations of long (minutes-to-years) GW transient from compact binaries, whose analysis is a formidable challenge for the years to come.

This work was funded by the Deutsche Forschungsgemeinschaft (DFG) under Grant No. 406116891 within the Research Training Group RTG 2522/1. S. B. acknowledge support by the EU H2020 under ERC Starting Grant, no. BinGraSp-714626. Data analysis was performed on the supercomputer ARA at Jena. We acknowledge the computational resources provided by Friedrich Schiller University Jena, supported in part by DFG grants INST 275/334-1 FUGG and INST 275/363-1 FUGG. Data postprocessing was performed on the Virgo "Tullio" server in Torino, supported by INFN. `TEOBResumS` and `TEOBResumSPA` are both publicly available at

`https://bitbucket.org/eob_ihes/teobresums/`

The data behind the figures and tables of this paper can be freely downloaded from

`https://doi.org/10.5281/zenodo.4476842`

This research has made use of data, software and/or web tools obtained from the Gravitational Wave Open Science Center (`https://www.gw-openscience.org`), a service of LIGO Laboratory, the LIGO Scientific Collaboration and the Virgo Collaboration. LIGO is funded by the U.S. National Science Foundation. Virgo is funded by the French Centre National de Recherche Scientifique (CNRS), the Italian Istituto Nazionale della Fisica Nucleare (INFN) and the Dutch Nikhef, with contributions by Polish and Hungarian institutes.

[1] J. Aasi et al. (LIGO Scientific), Class. Quant. Grav. **32**, 074001 (2015), arXiv:1411.4547 [gr-qc].
[2] F. Acernese et al. (VIRGO), Class. Quant. Grav. **32**, 024001 (2015), arXiv:1408.3978 [gr-qc].
[3] T. Damour, A. Nagar, and L. Villain, Phys.Rev. **D85**, 123007 (2012), arXiv:1203.4352 [gr-qc].
[4] S. Bernuzzi, A. Nagar, T. Dietrich, and T. Damour, Phys.Rev.Lett. **114**, 161103 (2015), arXiv:1412.4553 [gr-qc].
[5] M. Breschi, S. Bernuzzi, F. Zappa, M. Agathos, A. Perego, D. Radice, and A. Nagar, Phys. Rev. **D100**, 104029 (2019), arXiv:1908.11418 [gr-qc].
[6] P. Amaro-Seoane et al. (LISA), (2017), arXiv:1702.00786 [astro-ph.IM].
[7] M. A. Sedda et al., Class. Quant. Grav. **37**, 215011 (2020), arXiv:1908.11375 [gr-qc].
[8] S. Kawamura et al., (2020), arXiv:2006.13545 [gr-qc].
[9] A. Sesana, Phys. Rev. Lett. **116**, 231102 (2016), arXiv:1602.06951 [gr-qc].
[10] T. Damour, B. R. Iyer, and B. S. Sathyaprakash, Phys. Rev. **D57**, 885 (1998), arXiv:gr-qc/9708034 [gr-qc].
[11] T. Damour, B. R. Iyer, and B. Sathyaprakash, Phys.Rev. **D62**, 084036 (2000), arXiv:gr-qc/0001023 [gr-qc].
[12] T. Damour, B. R. Iyer, and B. S. Sathyaprakash, Phys. Rev. **D63**, 044023 (2001), [Erratum: Phys. Rev.D72,029902(2005)], arXiv:gr-qc/0010009 [gr-qc].
[13] A. Buonanno, B. Iyer, E. Ochsner, Y. Pan, and B. Sathyaprakash, Phys.Rev. **D80**, 084043 (2009), arXiv:0907.0700 [gr-qc].
[14] L. Blanchet, Living Rev. Relativity **17**, 2 (2014), arXiv:1310.1528 [gr-qc].
[15] A. Buonanno and T. Damour, Phys. Rev. **D59**, 084006 (1999), arXiv:gr-qc/9811091.
[16] A. Buonanno and T. Damour, Phys. Rev. **D62**, 064015 (2000), arXiv:gr-qc/0001013.
[17] T. Damour, P. Jaranowski, and G. Schaefer, Phys. Rev. **D62**, 084011 (2000), arXiv:gr-qc/0005034 [gr-qc].
[18] T. Damour, Phys. Rev. **D64**, 124013 (2001), arXiv:gr-qc/0103018.
[19] T. Damour, P. Jaranowski, and G. Schäfer, Phys.Rev. **D78**, 024009 (2008), arXiv:0803.0915 [gr-qc].
[20] T. Damour and A. Nagar, Phys. Rev. **D79**, 081503 (2009), arXiv:0902.0136 [gr-qc].
[21] T. Damour, P. Jaranowski, and G. Schäfer, Phys. Rev. **D91**, 084024 (2015), arXiv:1502.07245 [gr-qc].
[22] A. Bohé et al., Phys. Rev. **D95**, 044028 (2017), arXiv:1611.03703 [gr-qc].
[23] D. Bini, T. Damour, and A. Geralico, Phys. Rev. Lett. **123**, 231104 (2019), arXiv:1909.02375 [gr-qc].
[24] D. Bini, T. Damour, and A. Geralico, Phys. Rev. D **102**, 024062 (2020), arXiv:2003.11891 [gr-qc].
[25] D. Bini, T. Damour, and A. Geralico, Phys. Rev. D **102**, 024061 (2020), arXiv:2004.05407 [gr-qc].
[26] A. Nagar, G. Riemenschneider, G. Pratten, P. Rettegno, and F. Messina, (2020), arXiv:2001.09082 [gr-qc].
[27] S. Ossokine et al., (2020), arXiv:2004.09442 [gr-qc].
[28] M. Hannam, P. Schmidt, A. Bohé, L. Haegel, S. Husa, F. Ohme, G. Pratten, and M. Pürrer, Phys. Rev. Lett. **113**, 151101 (2014), arXiv:1308.3271 [gr-qc].
[29] S. Khan, S. Husa, M. Hannam, F. Ohme, M. Pürrer, X. Jiménez Forteza, and A. Bohé, Phys. Rev. **D93**, 044007 (2016), arXiv:1508.07253 [gr-qc].
[30] L. London, S. Khan, E. Fauchon-Jones, X. J. Forteza, M. Hannam, S. Husa, C. Kalaghatgi, F. Ohme, and F. Pannarale,

Phys. Rev. Lett. **120**, 161102 (2018), arXiv:1708.00404 [gr-qc].
[31] C. Garc´ia-Quirós, M. Colleoni, S. Husa, H. Estellés, G. Pratten, A. Ramos-Buades, M. Mateu-Lucena, and R. Jaume, Phys. Rev. D **102**, 064002 (2020), arXiv:2001.10914 [gr-qc].
[32] G. Pratten, S. Husa, C. Garcia-Quiros, M. Colleoni, A. Ramos-Buades, H. Estelles, and R. Jaume, Phys. Rev. D **102**, 064001 (2020), arXiv:2001.11412 [gr-qc].
[33] G. Pratten et al., (2020), arXiv:2004.06503 [gr-qc].
[34] P. Canizares, S. E. Field, J. Gair, V. Raymond, R. Smith, and M. Tiglio, Phys. Rev. Lett. **114**, 071104 (2015), arXiv:1404.6284 [gr-qc].
[35] R. Smith, S. E. Field, K. Blackburn, C.-J. Haster, M. Pürrer, V. Raymond, and P. Schmidt, Phys. Rev. **D94**, 044031 (2016), arXiv:1604.08253 [gr-qc].
[36] S. Morisaki and V. Raymond, Phys. Rev. D **102**, 104020 (2020), arXiv:2007.09108 [gr-qc].
[37] S. E. Field, C. R. Galley, F. Herrmann, J. S. Hesthaven, E. Ochsner, and M. Tiglio, Phys. Rev. Lett. **106**, 221102 (2011), arXiv:1101.3765 [gr-qc].
[38] M. Pürrer, Phys. Rev. **D93**, 064041 (2016), arXiv:1512.02248 [gr-qc].
[39] B. D. Lackey, S. Bernuzzi, C. R. Galley, J. Meidam, and C. Van Den Broeck, Phys. Rev. **D95**, 104036 (2017), arXiv:1610.04742 [gr-qc].
[40] J. Blackman, S. E. Field, M. A. Scheel, C. R. Galley, C. D. Ott, M. Boyle, L. E. Kidder, H. P. Pfeiffer, and B. Szilágyi, Phys. Rev. D **96**, 024058 (2017), arXiv:1705.07089 [gr-qc].
[41] B. D. Lackey, M. Pürrer, A. Taracchini, and S. Marsat, Phys. Rev. D **100**, 024002 (2019), arXiv:1812.08643 [gr-qc].
[42] V. Varma, S. E. Field, M. A. Scheel, J. Blackman, D. Gerosa, L. C. Stein, L. E. Kidder, and H. P. Pfeiffer, Phys. Rev. Research. **1**, 033015 (2019), arXiv:1905.09300 [gr-qc].
[43] R. Cotesta, S. Marsat, and M. Pürrer, Phys. Rev. D **101**, 124040 (2020), arXiv:2003.12079 [gr-qc].
[44] A. Nagar and P. Rettegno, Phys. Rev. **D99**, 021501 (2019), arXiv:1805.03891 [gr-qc].
[45] S. Akcay, S. Bernuzzi, F. Messina, A. Nagar, N. Ortiz, and P. Rettegno, Phys. Rev. **D99**, 044051 (2019), arXiv:1812.02744 [gr-qc].
[46] A. Nagar, F. Messina, P. Rettegno, D. Bini, T. Damour, A. Geralico, S. Akcay, and S. Bernuzzi, Phys. Rev. **D99**, 044007 (2019), arXiv:1812.07923 [gr-qc].
[47] P. Rettegno, F. Martinetti, A. Nagar, D. Bini, G. Riemenschneider, and T. Damour, (2019), arXiv:1911.10818 [gr-qc].
[48] T. Damour, in Gravitational Radiation, edited by N. Deruelle and T. Piran (North-Holland, Amsterdam, 1983) pp. 59–144.
[49] T. Hinderer, Astrophys.J. **677**, 1216 (2008), arXiv:0711.2420 [astro-ph].
[50] T. Damour and A. Nagar, Phys. Rev. **D80**, 084035 (2009), arXiv:0906.0096 [gr-qc].
[51] T. Binnington and E. Poisson, Phys. Rev. **D80**, 084018 (2009), arXiv:0906.1366 [gr-qc].
[52] E. E. Flanagan and T. Hinderer, Phys.Rev. **D77**, 021502 (2008), arXiv:0709.1915 [astro-ph].
[53] T. Damour and A. Nagar, Phys. Rev. **D81**, 084016 (2010), arXiv:0911.5041 [gr-qc].
[54] M. Favata, Phys.Rev.Lett. **112**, 101101 (2014), arXiv:1310.8288 [gr-qc].
[55] T. Damour and A. Nagar, Phys.Rev. **D90**, 044018 (2014), arXiv:1406.6913 [gr-qc].
[56] A. Nagar, G. Riemenschneider, and G. Pratten, Phys. Rev. **D96**, 084045 (2017), arXiv:1703.06814 [gr-qc].
[57] A. Nagar et al., Phys. Rev. **D98**, 104052 (2018), arXiv:1806.01772 [gr-qc].
[58] A. Nagar, G. Pratten, G. Riemenschneider, and R. Gamba, (2019), arXiv:1904.09550 [gr-qc].
[59] S. Bernuzzi, T. Dietrich, and A. Nagar, Phys. Rev. Lett. **115**, 091101 (2015), arXiv:1504.01764 [gr-qc].
[60] L. Lindblom, B. J. Owen, and D. A. Brown, Phys.Rev. **D78**, 124020 (2008), arXiv:0809.3844 [gr-qc].
[61] T. Damour, A. Nagar, and M. Trias, Phys. Rev. **D83**, 024006 (2011), arXiv:1009.5998 [gr-qc].
[62] K. Chatziioannou, A. Klein, N. Yunes, and N. Cornish, Phys. Rev. **D95**, 104004 (2017), arXiv:1703.03967 [gr-qc].
[63] R. Gamba, M. Breschi, S. Bernuzzi, M. Agathos, and A. Nagar, (2020), arXiv:2009.08467 [gr-qc].
[64] "LIGO Document T0900288-v3," `https://dcc.ligo.org/cgi-bin/DocDB/ShowDocument?docid=2974`, Advanced LIGO anticipated sensitivity curves.
[65] S. Husa, S. Khan, M. Hannam, M. Pürrer, F. Ohme, X. Jiménez Forteza, and A. Bohé, Phys. Rev. **D93**, 044006 (2016), arXiv:1508.07250 [gr-qc].
[66] T. Dietrich, S. Bernuzzi, and W. Tichy, Phys. Rev. **D96**, 121501 (2017), arXiv:1706.02969 [gr-qc].
[67] T. Hinderer et al., Phys. Rev. Lett. **116**, 181101 (2016), arXiv:1602.00599 [gr-qc].
[68] J. Steinhoff, T. Hinderer, A. Buonanno, and A. Taracchini, Phys. Rev. **D94**, 104028 (2016), arXiv:1608.01907 [gr-qc].
[69] B. P. Abbott et al. (LIGO Scientific, Virgo), Phys. Rev. **X9**, 011001 (2019), arXiv:1805.11579 [gr-qc].
[70] B. Abbott et al. (LIGO Scientific, Virgo), Astrophys. J. Lett. **892**, L3 (2020), arXiv:2001.01761 [astro-ph.HE].
[71] T. Robson, N. J. Cornish, and C. Liu, Class. Quant. Grav. **36**, 105011 (2019), arXiv:1803.01944 [astro-ph.HE].
[72] B. Zackay, L. Dai, and T. Venumadhav, (2018), arXiv:1806.08792 [astro-ph.IM].
[73] S. Vinciguerra, J. Veitch, and I. Mandel, Class. Quant. Grav. **34**, 115006 (2017), arXiv:1703.02062 [gr-qc].
[74] S. Schmidt, M. Breschi, R. Gamba, G. Pagano, P. Rettegno, G. Riemenschneider, S. Bernuzzi, A. Nagar, and W. Del Pozzo, (2020), arXiv:2011.01958 [gr-qc].
[75] B. P. Abbott et al. (Virgo, LIGO Scientific), Phys. Rev. Lett. **119**, 161101 (2017), arXiv:1710.05832 [gr-qc].
[76] B. P. Abbott et al. (GROND, SALT Group, OzGrav, DFN, INTEGRAL, Virgo, Insight-Hxmt, MAXI Team, Fermi-LAT, J-GEM, RATIR, IceCube, CAASTRO, LWA, ePESSTO, GRAWITA, RIMAS, SKA South Africa/MeerKAT, H.E.S.S., 1M2H Team, IKI-GW Follow-up, Fermi GBM, Pi of Sky, DWF (Deeper Wider Faster Program), Dark Energy Survey, MASTER, AstroSat Cadmium Zinc Telluride Imager Team, Swift, Pierre Auger, ASKAP, VINROUGE, JAGWAR, Chandra Team at McGill University, TTU-NRAO, GROWTH, AGILE Team, MWA, ATCA, AST3, TOROS, Pan-STARRS, NuSTAR,

ATLAS Telescopes, BOOTES, CaltechNRAO, LIGO Scientific, High Time Resolution Universe Survey, Nordic Optical Telescope, Las Cumbres Observatory Group, TZAC Consortium, LOFAR, IPN, DLT40, Texas Tech University, HAWC, ANTARES, KU, Dark Energy Camera GW-EM, CALET, Euro VLBI Team, ALMA), Astrophys. J. **848**, L12 (2017), arXiv:1710.05833 [astro-ph.HE].

[77] B. P. Abbott et al. (LIGO Scientific, Virgo), Phys. Rev. **X9**, 031040 (2019), arXiv:1811.12907 [astro-ph.HE].

[78] R. Smith and G. Ashton, (2019), arXiv:1909.11873 [gr-qc].

[79] I. Romero-Shaw et al., (2020), 10.1093/mnras/staa2850, arXiv:2006.00714 [astro-ph.IM].

[80] J. S. Speagle, Mon. Not. Roy. Astron. Soc. **493**, 3132 (2020), arXiv:1904.02180 [astro-ph.IM].

[81] M. Punturo, M. Abernathy, F. Acernese, B. Allen, N. Andersson, et al., Class.Quant.Grav. **27**, 084007 (2010).

[82] B. Sathyaprakash et al., in 46th Rencontres de Moriond on Gravitational Waves and Experimental Gravity (2011) pp. 127–136, arXiv:1108.1423 [gr-qc].

[83] M. Maggiore et al., JCAP **03**, 050 (2020), arXiv:1912.02622 [astro-ph.CO].

[84] D. Reitze et al., Bull. Am. Astron. Soc. **51**, 035 (2019), arXiv:1907.04833 [astro-ph.IM].

[85] S. Sato et al., J. Phys. Conf. Ser. **154**, 012040 (2009).

[86] We recall that Phenomenological approximants are based on fits to PN and EOB waveforms, and do not provide an independent description of this regime.

[87] Note that we do not simulate coalescences over the entire LISA frequency band, but focus only on the last hours/days of inspiral. This is due to the heavy computational burden represented by interpolating and working with waveforms evaluated on a frequency grid having $\Delta f \lesssim 1/\text{year}$.

[88] C. Cutler et al., (2019), arXiv:1903.04069 [astro-ph.HE].

[89] R. Gamba, S. Bernuzzi, and A. Nagar, "Fast, faithful, frequency-domain effective-one- body waveforms for compact binary coalescences," (2021).

[90] B. P. Abbott et al. (LIGO Scientific), Class. Quant. Grav. **34**, 044001 (2017), arXiv:1607.08697 [astro-ph.IM].

[91] M. Punturo, M. Abernathy, F. Acernese, B. Allen, N. Andersson, et al., Class.Quant.Grav. **27**, 194002 (2010).